A quantum relaxation-time approximation for finite fermion systems

P.-G. Reinhard*[1] and E. Suraud[2, 3, 4]

[1] *Institut für Theoretische Physik, Universität Erlangen, Staudtstraße 7, D-91058 Erlangen, Germany*
[2] *Université de Toulouse; UPS; Laboratoire de Physique Théorique, IRSAMC; F-31062 Toulouse Cedex, France*
[3] *CNRS; UMR5152; F-31062 Toulouse Cedex, France*
[4] *Physics Department, University at Buffalo, The State University New York, Buffalo, NY 14260, USA*

(Dated: September 16, 2014)

We propose a relaxation time approximation for the description of the dynamics of strongly excited fermion systems. Our approach is based on time-dependent density functional theory at the level of the local density approximation. This mean-field picture is augmented by collisional correlations handled in relaxation time approximation which is inspired from the corresponding semi-classical picture. The method involves the estimate of microscopic relaxation rates/times which is presently taken from the well established semi-classical experience. The relaxation time approximation implies evaluation of the instantaneous equilibrium state towards which the dynamical state is progressively driven at the pace of the microscopic relaxation time. As test case, we consider Na clusters of various sizes excited either by a swift ion projectile or by a short and intense laser pulse, driven in various dynamical regimes ranging from linear to strongly non-linear reactions. We observe a strong effect of dissipation on sensitive observables such as net ionization and angular distributions of emitted electrons. The effect is especially large for moderate excitations where typical relaxation/dissipation time scales efficiently compete with ionization for dissipating the available excitation energy. Technical details on the actual procedure to implement a working recipe of such a quantum relaxation approximation are given in appendices for completeness.

PACS numbers: 05.30.Fk,31.70.Hq,34.10.+x,36.40.Cg

arXiv:1409.4233v1 [physics.atm-clus] 15 Sep 2014

I. INTRODUCTION

The analysis of the non linear response of finite fermion systems subject to strong perturbations constitutes a central issue in many areas of physics. Prominent examples are low energy nuclear physics and fission [1, 2] as well as excitation of clusters and molecules by intense laser pulses [3, 4]. But similar situations are also encountered elsewhere, for example, in trapped Fermi gases [5] or electron transport in nano systems [6]. The case of irradiated clusters and molecules has become particularly interesting due to recent progress in experimental techniques at the side of photon sources [4, 7] as well as at the side of detection accessing more and more detailed information from the decaying system. Particularly useful observables are from the distributions of emitted electron (energy, angular distributions...) through elaborate imaging techniques such as Velocity Map Imaging (VMI) [8, 9]. These highly sophisticated measurements call for elaborate theoretical modeling to reconstruct the underlying dynamics of both the irradiation and de-excitation process. The choice of models ranges from a highly detailed quantum description to macroscopic rate equations [4]. Each one of these approaches is valid in a limited range of dynamical scenarios. The robust and rather versatile Time-Dependent Density Functional Theory (TDDFT), mostly realized at the level of the Time-Dependent Local-Density Approximation (TDLDA), [10–12] certainly provides one of the best compromises in the domain of quantum dynamics from the linear regime up to highly non-linear processes [4, 13, 14]. Still TDLDA basically remains a mean-field approach and misses by construction dissipative effects from electron-electron collisions which are expected to play a role in the course of violent excitation/de-excitation scenarios. This limits the range of applicability of TDLDA to moderate excitations and/or the entrance phase of the dynamics. There is thus a strong interest to extend TDLDA by collisional dynamics in order to push the limits farther out. It is the goal of this paper to investigate such an extension by including the effect of collisional correlations (or dynamical correlations). The notion of "collisional correlations" is taken from Fermi liquid theory [15] with incoherent reduction of two-body correlations to two-Fermion collisions. As first example of application, we discuss the case of irradiated metal clusters. But we emphasize that the strategy outlined here is applicable to any many-fermion system where TDLDA is a good starting point, namely where it provides a good description of low energy dynamics.

The much celebrated Boltzmann equation constitutes the prototype approach to collisional dynamics in classical systems [16]. In quantum systems, one has to account for the Heisenberg uncertainty relation and the Pauli principle. Pauli blocking can be accounted for by extending the Boltzmann collision term to the Boltzmann-Uehling-Uhlenbeck (BUU) form [17]. This semi-classical BUU approach (also known as Vlasov-Uehling-Uhlenbeck (VUU) equation) provides an acceptable picture at sufficiently large excitations where quantum shell effects can be ignored. It has been extensively used in nu-

*Corresponding author : Paul-Gerhard.Reinhard@fau.de

clear physics [18, 19] and also explored in metal clusters [20, 21] in a high excitation domain. A further limitation of the BUU/VUU approach appears in the case of clusters: it is not clear that it could be used in systems others than simple alkalines, where electron wave functions are sufficiently delocalised and smooth to allow a semi-classical treatment [22]. This hinders, e.g., an application to C_{60} which is one of the systems attracting the most elaborate analysis of dissipative dynamics so far [7, 23]. It should finally be noted that even in the high-excitation domain a major de-excitation channel is ionization which may quickly take away large amounts of excitation energy cooling the system down into a regime where quantum effects cannot be neglected any more. This limits BUU/VUU often to the initial stages of a dynamical process. All this shows that there is an urgent need for a quantum description augmented by relaxation effects.

In spite of their limitations, semi-classical approaches nevertheless provide extremely useful guidance in three major aspects. First, they constitute a long standing testing basis for strategies to implement approximate relaxation pictures into a quantum framework [24]. Second, as we shall exploit below, they serve as source of inspiration for developing simple approximations for collisional relaxation in TDLDA. Last, but not least, they deliver approved estimates for the key quantities (collision rate, intrinsic relaxation time) to be used in quantum approximations.

The aim of this paper is to propose an extension of (real-time) TDLDA by collisional correlations. We shall exploit the experience from semi-classical approximations but keep the level of description quantum mechanical throughout. The paper is organized as follows. Section II provides the basics of the mean field description and introduces associated notations. Section III describes the proposed scheme for the Relaxation Time Approximation (RTA) and details of its handling. First results for the case of metal clusters are then presented in section IV and conclusions and perspectives are drawn in section V. Finally, the text is completed by a series of appendices which give some technical details on the RTA and its handling in practice.

II. MEAN-FIELD PROPAGATION

The starting point and dominant feature of the dynamics is the propagation at the level of the mean field. In this paper, we are dealing with the electron dynamics in metal clusters and we describe it by time-dependent density functional theory at the level of the Time-Dependent Local-Density Approximation (TDLDA) treated in the real time domain [10, 11]. It is augmented by a self-interaction correction (SIC) approximated by average-density SIC (ADSIC) [25] in order to attain correct ionization properties [26] in the course of the dynamical simulation. TDLDA is formulated within the usual Kohn-Sham picture in terms of a set of occupied single-particle (s.p.) wavefunctions $\{|\phi_\alpha\rangle, \alpha = 1...N\}$. Their dynamics is described by the time-dependent Kohn-Sham equation

$$\mathrm{i}\partial_t|\phi_\alpha\rangle = \hat{h}[\varrho]|\phi_\alpha\rangle \tag{1}$$

where $\hat{h}$ is the Kohn-Sham mean-field Hamiltonian which is a functional of the instantaneous local density $\varrho(\mathbf{r},t) = \sum_\alpha |\phi_\alpha(\mathbf{r},t)|^2$ [27, 28]. The time evolution delivered by Eq. (1) can be expressed formally by the unitary one-body time-evolution operator

$$\hat{U}(t,t') = \hat{\mathcal{T}}\exp\left(-i\int_t^{t'}\hat{h}(t'')dt''\right) \tag{2a}$$

where $\hat{\mathcal{T}}$ is the time-ordering operator. This yields a closed expression for the time-evolution of s.p. states

$$|\phi_\alpha(t)\rangle = \hat{U}(t,t')|\phi_\alpha(t')\rangle. \tag{2b}$$

So far, TDLDA propagates pure states. Dissipation which we will add later on leads inevitably to mixed states. This requires to generalize the description from fully occupied s.p. wavefunctions to a one-body density operator $\hat{\rho}$. It is often denoted as one-body density matrix $\rho(\mathbf{r},\mathbf{r}')$ which is, in fact, the coordinate representation of $\hat{\rho}$. A (natural orbitals) representation of the one-body density operator in terms of s.p. wavefunctions reads

$$\hat{\rho} = \sum_{\alpha=1}^{\infty}|\phi_\alpha\rangle W_\alpha\langle\phi_\alpha| \quad . \tag{3}$$

New are here the weights W_α, the probability with which a state $|\phi_\alpha\rangle$ is occupied. The mean-field propagation (1) then becomes

$$\mathrm{i}\partial_t\hat{\rho} = \left[\hat{h}[\varrho],\hat{\rho}\right] \tag{4}$$

where $\hat{h}[\varrho]$ is formally the same as before and the local density is now computed as

$$\varrho(\mathbf{r},t) = \sum_\alpha W_\alpha|\phi_\alpha(\mathbf{r},t)|^2. \tag{5}$$

The pure mean-field propagation (4) leaves the occupation weights W_α unchanged and propagates only the s.p. states. The mean-field propagation of an initial state (3) then reads

$$\begin{aligned}\hat{\rho}(t) &= \sum_{\alpha=1}^{\infty}|\phi_\alpha(t)\rangle W_\alpha\langle\phi_\alpha(t)| \\ &= \hat{U}(t,0)\hat{\rho}(0)\hat{U}^{-1}(t,0)\end{aligned} \tag{6}$$

where $\hat{U}$ is the mean-field evolution operator (2a).

III. THE RELAXATION-TIME APPROXIMATION (RTA) FOR FINITE FERMION SYSTEMS

A. Motivation: RTA in a semi-classical framework

In homogeneous fermion systems the phase space distribution f only depends on momentum and dynamical correlations can be described by the Uehling-Uhlenbeck collision term $I_{\rm UU}[f(\mathbf{p})]$ [17, 29]. It is a functional of the momentum space distribution $f(\mathbf{p})$ which drives the dynamics steadily towards the thermal equilibrium distribution $f_{\rm eq}$. As the collision term $I_{\rm UU}$ conserves particle number, mean momentum and energy, the $f_{\rm eq}(\mathbf{p};\varrho,\mathbf{j},E)$ represents the equilibrium for given density ϱ, current $\mathbf{j}$, and kinetic energy E. Sufficiently close to equilibrium, one can approximate the convergence as exponential relaxation which allows to model the dynamical process simply as

$$\partial_t f(\mathbf{p},t) = -\tau_{\rm relax}^{-1}\left(f(\mathbf{p},t) - f_{\rm eq}(\mathbf{p};\varrho,\mathbf{j},E)\right) \qquad (7)$$

where $\tau_{\rm relax}$ is the relaxation time. The expectation values $\varrho,\mathbf{j},E$ for density, current, and energy are the ones associated to $f(\mathbf{p},t)$ and computed as $\varrho = \int d^3p\, f(\mathbf{p},t)$, $\mathbf{j} = \int d^3p\, \mathbf{p}\, f(\mathbf{p},t)$, and $E = \int d^3p\, \mathbf{p}^2\, f(\mathbf{p},t)/(2m)$. This is called the Relaxation Time Approximation (RTA). It was introduced in [30] and it has been used used in that form for a wide variety of homogeneous systems [29, 31].

Finite fermion systems are spatially inhomogeneous. An obvious generalization to this case is to extend $f(\mathbf{p})$ to a phase-space distribution $f(\mathbf{r},\mathbf{p})$. This leads to a semi-classical description which is valid for high excitations (or temperatures) where quantum shell effects are obsolete. The mean-field dynamics is then described by the Vlasov equation and the dynamical correlations by an additional collision term $I_{\rm UU}[f(\mathbf{r},\mathbf{p})]$ yielding together the Vlasov-Uehling-Uhlenbeck (VUU) equation [32]

$$\partial_t f - \{h,f\} = I_{\rm UU}[f(\mathbf{r},\mathbf{p})] \qquad (8)$$

where h is the (classical) mean field Hamiltonian. In this semi-classical approach, collisions are local, changing for a given $\mathbf{r}$ only the momentum distribution at this point. It thus establishes local conservation laws [33] such that collisional relaxation conserves local density $\varrho(\mathbf{r},t)$, local current $\mathbf{j}(\mathbf{r},t)$, and local kinetic energy $E_{\rm kin}(\mathbf{r},t)$. The collision term thus drives towards a local and instantaneous equilibrium $f_{\rm eq}(\mathbf{r},\mathbf{p};\varrho,\mathbf{j},E_{\rm kin})$. The global equilibration is achieved at slower pace by interplay with the long range transport described by the mean-field propagation (Vlasov part of the VUU equation). The RTA for the VUU equation (8) reads [30, 34–36]

$$\partial_t f - \{h,f\} = -\frac{1}{\tau_{\rm relax}}\left(f(\mathbf{r},\mathbf{p},t) - f_{\rm eq}(\mathbf{r},\mathbf{p};\varrho,\mathbf{j},E_{\rm kin})\right) \qquad (9)$$

where the constraints $\varrho,\mathbf{j},E_{\rm kin}$ depend on position $\mathbf{r}$ and time t. This is the model which we will now generalize to the case of quantum mean-field theory.

B. RTA in quantum-mechanical framework

The generalization of the one-body phase-space distribution $f(\mathbf{r},\mathbf{p})$ to a quantum-mechanical mean-field theory is the one-body density operator $\hat\rho$, or one-body density matrix $\rho(\mathbf{r},\mathbf{r}')$ respectively. The equation of motion for $\hat\rho$ including dynamical correlations reads in general [37, 38]

$$\mathrm{i}\partial_t\hat\rho - \left[\hat h,\hat\rho\right] \;=\; \hat I[\hat\rho] \quad . \qquad (10)$$

The left hand side embraces the mean-field propagation. It may be time-dependent Hartree-Fock or the widely used LDA version of TDDFT. The right-hand side consists in the quantum-mechanical collision term. Motivated by the successful semi-classical RTA, we import Eq. (9) for the quantum case as

$$\partial_t\hat\rho \;=\; -\mathrm{i}\left[\hat h,\hat\rho\right] - \frac{1}{\tau_{\rm relax}}\left(\hat\rho - \hat\rho_{\rm eq}[\varrho,\mathbf{j},E]\right) \;, \qquad (11)$$

where $\hat\rho_{\rm eq}$ is the density operator of the thermal equilibrium for local density $\varrho(\mathbf{r},t)$, current distribution $\mathbf{j}(\mathbf{r},t)$ and total energy $E(t)$ given at that instant of time t. These constraining conditions are, in fact, functionals of the actual state $\hat\rho$, i.e. $\varrho[\hat\rho]$, $\mathbf{j}[\hat\rho]$, and $E[\hat\rho]$. For the diagonal representation Eq.(3) of the density operator $\hat\rho$, they read

$$\varrho(\mathbf{r}) \;=\; \sum_\alpha |\phi_\alpha(\mathbf{r})|^2\, W_\alpha \quad , \qquad (12a)$$

$$\mathbf{j}(\mathbf{r}) \;=\; \sum_\alpha W_\alpha \phi_\alpha^*(\mathbf{r}) \frac{\overrightarrow{\nabla} - \overleftarrow{\nabla}}{2\mathrm{i}} \phi_\alpha(\mathbf{r}) \quad . \qquad (12b)$$

The energy $E(t)$ is taken as the total energy because the semi-classical concept of a local kinetic energy is ambiguous in a quantum system. This RTA equation (11) looks innocent, but is very involved because many entries depend in various ways on the actual state $\hat\rho(t)$. The self-consistent mean field is a functional of the actual local density, i.e. $\hat h = \hat h[\varrho]$. The instantaneous equilibrium density $\hat\rho_{\rm eq}$ is the solution of the stationary, thermal mean-field equations with constraint on the actual $\varrho(\mathbf{r})$, $\mathbf{j}(\mathbf{r})$ and energy E, for details see Appendix B.

The relaxation time $\tau_{\rm relax}$ is estimated in semi-classical Fermi liquid theory, for details see appendix A 2. For the metal clusters serving as test examples in the following, it becomes

$$\frac{\hbar}{\tau_{\rm relax}} = 0.40 \frac{\sigma_{ee}}{r_s^2} \frac{E^*_{\rm intr}}{N} \quad , \qquad (13)$$

where $E^*_{\rm intr}$ is the intrinsic (thermal) energy of the system (appendix C), N the actual number of particles, σ_{ee} the in-medium electron-electron cross section, and r_s the effective Wigner-Seitz radius of the electron cloud.

C. Summary of the procedure

The solution of the RTA equations is rather involved. We explain the necessary steps here from a practical side

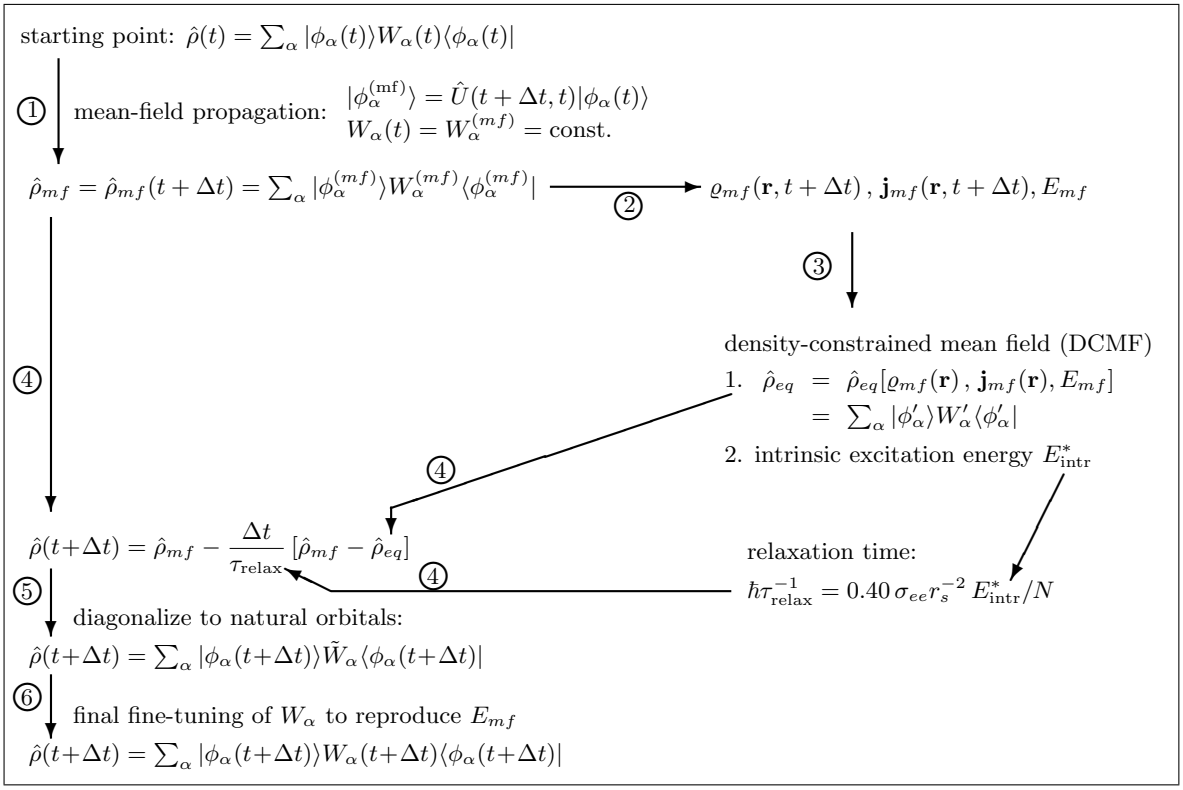
starting point: $\hat\rho(t) = \sum_\alpha |\phi_\alpha(t)\rangle W_\alpha(t) \langle\phi_\alpha(t)|$
①
mean-field propagation: $|\phi_\alpha^{(\rm mf)}\rangle = \hat U(t+\Delta t, t)|\phi_\alpha(t)\rangle$
$W_\alpha(t) = W_\alpha^{(mf)} = \text{const.}$
$\hat\rho_{mf} = \hat\rho_{mf}(t+\Delta t) = \sum_\alpha |\phi_\alpha^{(mf)}\rangle W_\alpha^{(mf)} \langle\phi_\alpha^{(mf)}|$
②
$\varrho_{mf}(\mathbf{r}, t+\Delta t)\,,\, \mathbf{j}_{mf}(\mathbf{r}, t+\Delta t), E_{mf}$
③
density-constrained mean field (DCMF)
1. $\hat\rho_{eq} = \hat\rho_{eq}[\varrho_{mf}(\mathbf{r})\,,\, \mathbf{j}_{mf}(\mathbf{r}), E_{mf}]$
$= \sum_\alpha |\phi'_\alpha\rangle W'_\alpha \langle\phi'_\alpha|$
2. intrinsic excitation energy $E^*_{\rm intr}$
④
④
$\hat\rho(t+\Delta t) = \hat\rho_{mf} - \dfrac{\Delta t}{\tau_{\rm relax}} [\hat\rho_{mf} - \hat\rho_{eq}]$
relaxation time:
④
$\hbar\tau^{-1}_{\rm relax} = 0.40\, \sigma_{ee} r_s^{-2}\, E^*_{\rm intr}/N$
⑤
diagonalize to natural orbitals:
$\hat\rho(t+\Delta t) = \sum_\alpha |\phi_\alpha(t+\Delta t)\rangle \tilde W_\alpha \langle\phi_\alpha(t+\Delta t)|$
⑥
final fine-tuning of W_α to reproduce E_{mf}
$\hat\rho(t+\Delta t) = \sum_\alpha |\phi_\alpha(t+\Delta t)\rangle W_\alpha(t+\Delta t) \langle\phi_\alpha(t+\Delta t)|$

Figure 1: Sketch of the scheme for performing one large time step $t \longrightarrow t+\Delta t$ in solving the RTA equations. The numbers in open circles indicate the steps as outlined in the text.

and unfold details in the appendices. We briefly summarize the actual scheme for one step from t to $t+\Delta t$. Note that mean-field propagation (actually TDLDA) runs at a much faster pace than relaxation. We resolve it by standard techniques [13, 28] on a time step δt which is much smaller (factor 10–100) than the RTA step Δt. We summarize this TDLDA propagation in the evolution operator $\hat U$ from Eq. (2a) and discuss only one RTA step. Its sub-steps are sketched in Figure 1 and explained in the following whereby the label here correspond to the ones in the Figure:

1. We first propagate $\hat\rho$ by pure TDLDA. This means that the s.p. states in representation (3) evolve as $|\phi_\alpha(t)\rangle \to |\phi_\alpha^{(\rm mf)}\rangle = \hat U(t+\Delta t, t)|\phi_\alpha(t)\rangle$, while the occupation weights W_α are kept frozen (pure mean-field propagation).

2. We compute density $\varrho(\mathbf{r}, t+\Delta t)$, current $\mathbf{j}(\mathbf{r}, t+\Delta t)$, and total energy $E_{\rm mf}$ associated to the TDLDA-propagated density matrix $\hat\rho_{\rm mf}$.

3. We determine the thermal mean-field equilibrium state $\hat\rho_{\rm eq}$ constrained to the given ϱ, $\mathbf{j}$, and $E_{\rm mf}$. This is achieved by Density-Constrained Mean Field (DCMF) iterations as outlined in Appendix B. The actual equilibrium state $\hat\rho_{\rm eq}$ is represented by new s.p. states $\{|\phi'_\alpha\rangle\}$ and new occupation numbers W'_α in diagonal form (3).

4. We compose the new density matrix from the TDLDA propagated state $\hat\rho_{\rm mf}$ and the equilibration driving term $\hat\rho_{\rm mf} - \hat\rho_{\rm eq}$ with the appropriate weight $\Delta t/\tau_{\rm relax}$, as outlined in Appendix D. The relaxation time Eq. (13) requires the actual intrinsic excitation energy $E^*_{\rm intr}$ which is also obtained from DCMF, see appendix C.

5. We diagonalize the state emerging from step 4 to natural-orbital representation Eq. (3). This yields the s.p. states $\{|\phi_\alpha(t+\Delta t)\rangle\}$ for the next step and preliminary new occupations $\tilde W_\alpha$.

6. After all these steps, the initial energy $E_{\rm mf} = E_{\rm TDLDA}(t)$ may not be exactly reproduced. We may remain with a small energy mismatch as compared to the goal $E_{\rm mf}$. We now apply a small iterative thermalization step to readjust the energy, as outlined in Appendix E. This then yields the final occupation weights $W_\alpha(t+\Delta t)$ which comply with energy conservation.

The scheme can be used also in connection with absorbing boundary conditions [13, 39]. The particle loss will be mapped automatically to loss of occupation weights in step 4. A word is in order about the choice of the time steps. The δt for propagation of TDLDA is limited by the maximal energy on the grid representation and thus very

small (for Na clusters typically 0.005 fs). The stepping for the relaxation term needs only to resolve the changes in the actual mean field which is achieved already with $\Delta t \approx 0.5$ fs. We have tested a sequence of Δt and find the same results for all $\Delta t \leq 0.5$ fs. Changes appear slowly above that value. For reasons of efficiency, we thus use the largest safe value of $\Delta t = 0.5$ fs.

D. Numerical representation and computation of relevant observables

The numerical implementation of TDLDA is done in standard manner [13, 28]. The coupling to the ions is mediated by soft local pseudopotentials [40]. The Kohn-Sham potential is handled in the Cylindrically Averaged Pseudo-potential Scheme (CAPS) [41, 42], which has proven to be an efficient and reliable approximation for metal clusters close to axial symmetry. Wavefunctions and fields are thus represented on a 2D cylindrical grid in coordinate space [43]. For the typical example of the Na_{40} cluster, the numerical box extends up to 104 a_0 in radial direction and 208 a_0 along the z-axis, while the grid spacing is 0.8 a_0. To solve the (time-dependent) Kohn-Sham equations (1) we use time-splitting for time propagation [44] and accelerated gradient iterations for the stationary solution [45]. The Coulomb field is computed with successive over-relaxation [43]. We use absorbing boundary conditions [13, 39], which gently absorb all outgoing electron flow reaching the bounds of the grid and thus prevent artifacts from reflection back into the reaction zone. We take the exchange-correlation energy functional from Perdew and Wang [46].

A great manifold of observables can be deduced from the $\hat{\rho}(t)$ thus obtained. We will consider in the following the dipole signal, dipole spectrum, ionization, angular distribution of emitted electrons, and entropy. We focus here on the dipole moment along symmetry axis z, which is obtained from the local density as $\langle \hat{d}_z \rangle(t) = \int d^3r \, d_z(\mathrm{z}) \varrho(\mathrm{r})$ where $d_z(\mathrm{z}) = z$ is the (local) dipole operator. The dipole strength distribution is computed with the methods of spectral analysis [47]. It is attained by an instantaneous dipole-boost excitation, collecting $\langle \hat{d}_z \rangle(t)$ during propagation, and finally Fourier transforming $\langle \hat{d}_z \rangle(t)$ into frequency domain. The angular distribution of emitted electrons is obtained from recording the absorbed electrons as in TDLDA [48, 49]. The angular distribution is characterized by the anisotropy parameter β_2, the leading parameter in the photo-electron angular cross section $d\sigma/d\Omega \propto (1 + \beta_2 P_2(cos(\theta) + ...)$ [50, 51] where P_2 is the second order Legendre polynomial and θ the direction with respect to laser polarization axis (here z-axis in 2D cylindrical geometry). A specific quantity to track relaxation processes is the one-body entropy which is computed in diagonal representation (3) by the standard expression [52]

$$S = -\sum_{\alpha} [W_\alpha \log W_\alpha + (1-W_\alpha)\log(1-W_\alpha)] \qquad (14)$$

in units of Bolzmann constant. It serves as a direct indicator of thermalization and allows to read off the typical time scale of relaxation processes.

IV. RESULTS

A. The test cases

As test cases, we will consider the clusters, Na_{40}, Na_9^+, Na_{41}^+, and Na_{93}^+. All test cases have electronic shell closures ($N_{\mathrm{el}} = 8, 40, 92$ [53]) and are thus close to spherical symmetry. This is no principle restriction because computations with deformed systems show similar pattern. In fact, shell closures with their large HOMO-LUMO gaps are the most demanding situations (thus critical test cases) for the RTA scheme. The ionic ground-state configuration is optimized by iterative cooling in the spirit of simulated annealing [13, 28]. In the following we are interested exclusively in electronic dissipation and we are considering rather short time intervals. We thus keep the ions frozen at their ground-state configurations. The Wigner-Seitz radius required in the estimate of local relaxation time Eq. (13) is computed with the recipes of Appendix A 2. It turns out to be almost the same for all test cases mentioned above. We use in practice $r_s = 3.7$ a_0. The TDLDA equations are propagated with a time step of $\delta t = 0.005$ fs. The larger time step for evaluation of the dissipative term is $\Delta t = 0.5$ fs.

B. Trends for boost excitations

In the first round, we use the simplest excitation mechanism to elucidate the basic effects of dissipative term. This is an instantaneous dipole boost $\phi_\alpha \rightarrow \exp(-\mathrm{i}\, p_0 \hat{d}_z)\phi_\alpha$ applied to all s.p. wavefunctions in the same manner [13, 28]. The boost momentum p_0 regulates its strength. We are characterizing the boost strength henceforth in terms of the initial excitation energy $E_0^* = Np_0^2/(2m)$ brought into the cluster by the boost. Mind that E_0^* is the *initial* excitation energy deposited into the system, not to be confused with the time dependent intrinsic excitation energy E_{intr}^* used in estimating the relaxation time (13). The instantaneous dipole boost models to a good approximation the time-dependent Coulomb field at the cluster site for collisions with very fast ion passing by the cluster [54, 55].

1. *Optical response as initial example*

Optical response is the basic observable characterizing the reaction of a cluster to an electromagnetic perturba-

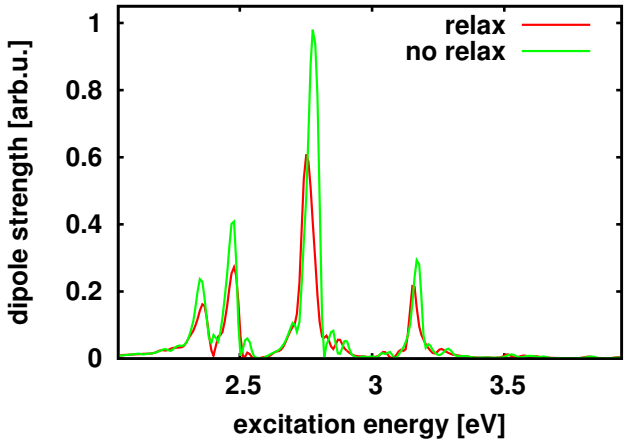

Figure 2: (Color online) Spectral distribution of dipole strength for Na_{40} with ionic background in the CAPS, evaluated for a boost strength $E_0^* = 2.7$ eV according to the scheme of [47]. Compared are calculations with and without relaxation term.

tion and it serves as key to the analysis of a large variety of dynamical scenarios [28]. It is thus of interest to check the impact of RTA on optical response. We take here Na_{40} as test example. Its optical response is dominated by a surface plasmon resonance in a rather narrow spectral range around 2.7 eV.

Figure 2 shows the effect of dissipation on the spectral distribution of dipole strength for an excitation in the one-plasmon regime, i.e. $E_0^* = 2.7$ eV. The spectra are computed after instantaneous boost with spectral analysis of the dipole signal [47]. As expected, the relaxation term leads to broadening of the spectral peaks because the lifetime of the eigenmodes is reduced by dissipation. However, the effect is surprisingly small. This is due to the competition with an even stronger relaxation through direct electronic emission. This mechanism is contained in TDLDA and has already achieved a great deal of smoothing the peaks leaving little to do for collisional relaxation. But mind that this competition between direct emission and collisional relaxation depends sensitively on the actual details of the system and excitation mechanisms, especially on the total amount of deposited excitation energy E_0^*.

2. *Trends with varied excitation strength*

Figure 3 shows the time evolution of relative ionization $N_{\rm esc}/E_0^*$, envelope of the dipole signal $\langle \hat{d}_z \rangle$, entropy S, and anisotropy β_2 for Na_{40} after boosts with different strengths. Results from pure TDLDA are shown with dotted lines and those including dissipation with full lines. The three cases for E_0^* represent three regimes: linear response for $E_0^* = 0.27$ eV, the one-plasmon regime for $E_0^* = 2.7$ eV, and the three-plasmon (non-linear) regime for $E_0^* = 8.1$ eV.

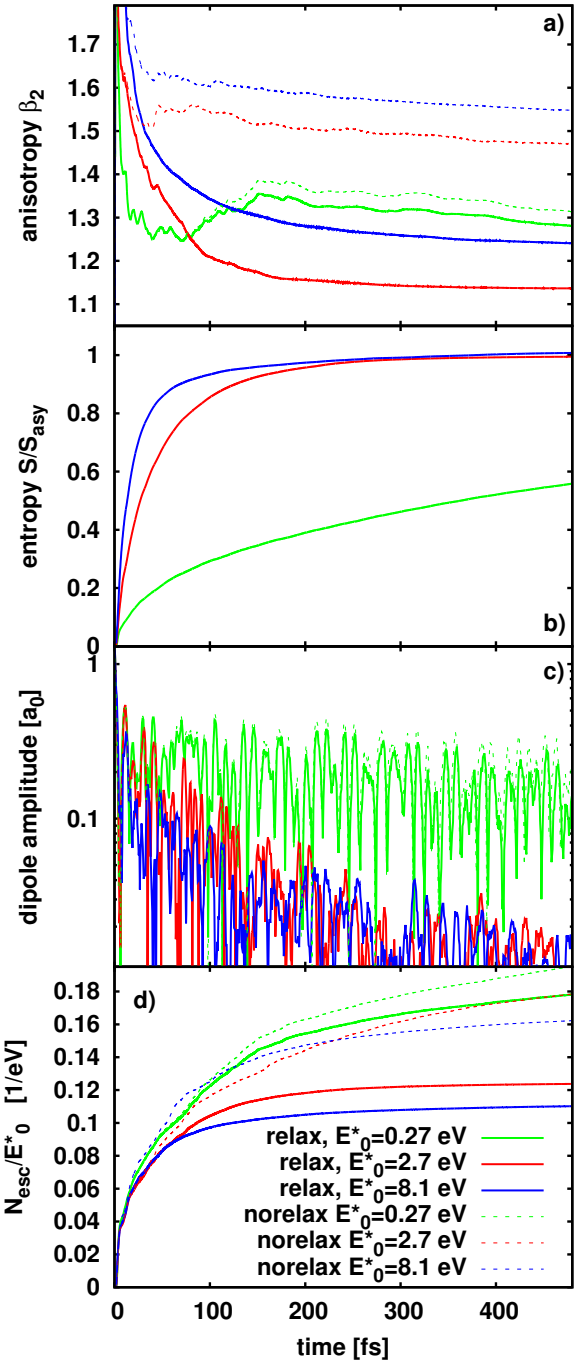

Figure 3: (Color online) Time evolution of four key observables after an instantaneous boost with three different boost energies as indicated. Test case is Na_{40} with ionic background in the CAPS. The observables are: d) ionization $N_{\rm esc}/E_0^*$ rescaled to initial excitation energy E_0^*, c) envelope of the dipole signal $\langle \hat{d}_z \rangle$, b) entropy S relative to the asymptotic value $S_{\rm asy}$, and a) anisotropy β_2 of the angular distribution of emitted electrons. The cases with relaxation are drawn with full lines and computed with the standard scattering cross section $\sigma_{ee} = 6.5$ a_0^2. TDLDA results are drawn with dotted lines.

The dipole amplitudes (panel c) are shown in logarithmic scale to visualize the long-time trend. They decay with time, the faster the higher the excitation E_0^*. Even the envelope of the dipole signal is heavily fluctuating such that it is hard to read off a global relaxation time. Moreover, already the TDLDA amplitudes are attenuated due to Landau damping and direct electron emission [13, 28]. The dissipative effect corresponds to the difference between TDLDA and RTA propagation. Unfortunately, it cannot be extracted cleanly from the dipole signal.

The entropy, Eq. (14), stays at $S = 0$ for pure TDLDA. It is thus a selective signal for dissipative effects and only results from the RTA calculations are relevant here. Panel b in Figure 3 shows the entropy relative to the asymptotic value to allow a direct comparison of the three cases. All three cases show a nice exponential convergence. The corresponding global relaxation time depends sensitively on the excitation energy E_0^*. There is practically no dissipation for the faintest excitation. This is clear from the recipe Eq. (13) for the local relaxation rate which is $\propto E_0^*$ and thus disappears for $E_0^* \to 0$. Dissipation increases with increasing excitation amounting to a global relaxation time of about 50 fs for the one-plasmon regime $E_0^* = 2.7$ eV and to 25 fs for $E_0^* = 8.1$ eV.

Dissipation has a large effect on ionization (panel d). For TDLDA, the leading damping mechanism in the late phase is electron emission and this continues for long as one can see from the slowly but continuously growing $N_{\rm esc}$, accompanied by slowly decreasing dipole amplitude. Dissipation offers an alternative channel for damping, namely internal excitation. Consequently, ionization is much suppressed, the more the stronger dissipation is at work, i.e. practically not for $E_0^* = 0.27$ eV and increasing with E_0^*.

Anisotropy is a well known signal of thermalization. Angular distributions become more and more isotropic the more thermalized a system is. It is thus important to compare TDLDA with RTA in that respect. This is done in panel a of Figure 3. Dissipation clearly leads to a reduction of β_2. It is, nevertheless, interesting to note the counteracting effects pulling on β_2, one due to TDLDA, the other one to RTA. The trend is simple for pure TDLDA: the stronger the boost the larger the drive to forward/backward emission and thus the larger β_2. On the other hand, larger excitation enhances dissipation and reduces increasingly β_2. Eventually, the trend can go both ways.

Finally, remind that the analysis of angular distributions is done here over finite times which means that the β_2 shown here are not yet the asymptotic values. The excitation energy stored in intrinsic degrees of freedom by dissipation will be released slowly later, to a large extent in terms of thermal electron emission. This adds an isotropic background of thermal electrons which will further reduce the anisotropy. A strategy to estimate this effect is proposed in [55, 56]. We skip this final clean-up in the present exploratory study as it is not crucial for understanding RTA.

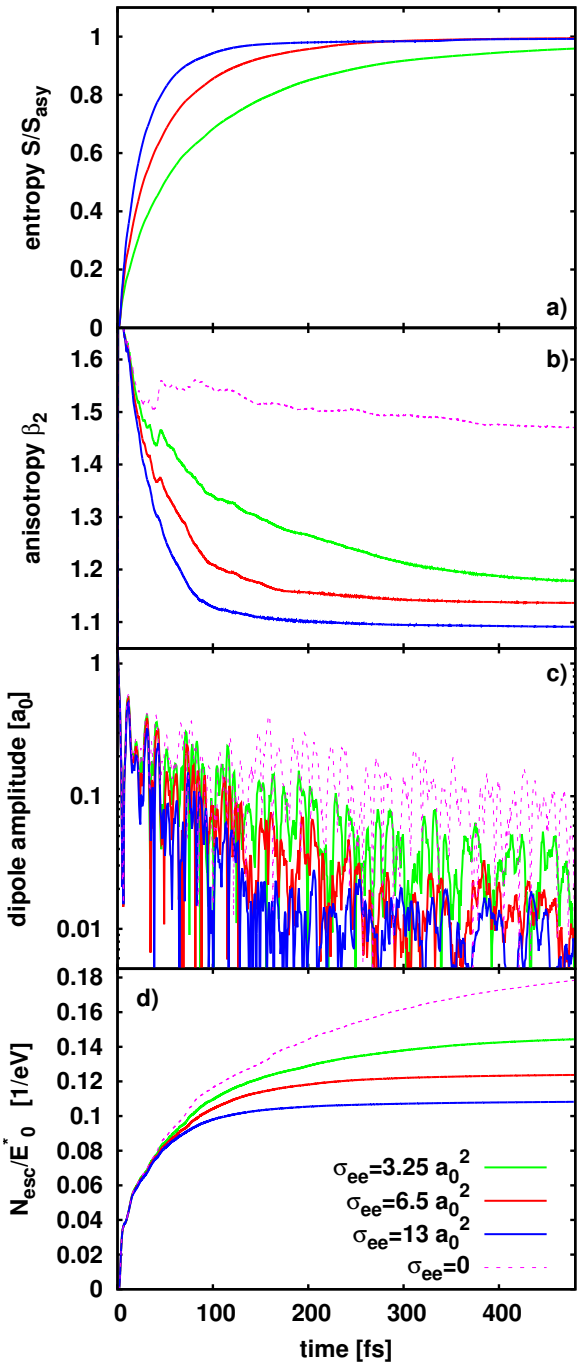

Figure 4: (Color online) Same as Fig. 3, but for varied cross sections σ_{ee} defining $\tau_{\rm relax}$ which correspond to the standard $\sigma_{ee} = 6.5$ a$_0^2$ and half as well as twice that value. The boost energy is $E_0^* = 2.7$ in all cases.

3. Trends with electron-electron cross section

The choice of the cross section σ_{ee} for in-medium electron scattering is, of course, a crucial ingredient for the estimate of the relaxation time Eq. (13). To explore the sensitivity on the choice of σ_{ee}, we show in Figure 4 results for three values of σ_{ee} in steps of factors 2, namely for the standard value of $\sigma_{ee} = 6.5\ a_0^2$ (see appendix A 2) used in most of the paper, and for 13 a_0^2 (twice that cross section), and for 3.25 a_0^2 (half of it). The comparison is done for the one-plasmon excitation regime $E_0^* = 2.7$ eV. The effects of varying σ_{ee} are large. From the entropy signal (panel a), we can read off that the global relaxation time shrinks here almost inversely proportional to the cross section, from 100 fs over 50 fs down to about 25 fs. One can spot the same trend in the attenuation of the dipole signal in panel c. Correspondingly, we see an increasing suppression of ionization with increasing cross section. In this case, however, the changes are more moderate, far slower than proportional. The same holds for the anisotropy (panel b). Reduction of β_2 increases with σ_{ee}, but rather slowly.

It is to be noted that the excitation of $E_0^* = 2.7$ eV chosen here is the most sensitive case for variation of σ_{ee} around the standard choice. Very little happens, of course, deep in the linear regime where dissipation is negligible anyway. Somewhat less sensitivity is also seen for heftier excitations (not shown here).

4. Trends with system size

The next question is how dissipative effects depend on charge state and system size. Figure 5 shows results for three cluster cations of different size, Na_9^+, Na_{41}^+, and Na_{93}^+, all with the same excitation $E_0^* = 2.7$ eV in the one-plasmon regime. Comparison of Na_{41}^+ here in Figure 5 with the case of $E_0^* = 2.7$ eV for Na_{40} in Figure 3 shows that one more charge changes very little in all respects (emission, dipole amplitude, relaxation time, anisotropy). However, system size makes a huge difference. The smaller system Na_9^+ has much stronger dissipative effects (shorter relaxation time, more suppression of ionization) while the heavier cluster Na_{93}^+ shows very small relaxation. A quick glance at recipe (13) for the relaxation rate explains this. The rate is proportional to $E^*_{\rm intr}/N$. Large electron number N thus reduces the rate while low N enhances it. The effect is obvious: the plasmon energy depends only weakly on system size [57] but the thermal effects are related to the energy per particle. The latter quantity shrinks with increasing size. As a consequence, a one-plasmon excitation remains safely in the linear regime for heavy clusters while small clusters experience more thermal effects as, e.g., relaxation.

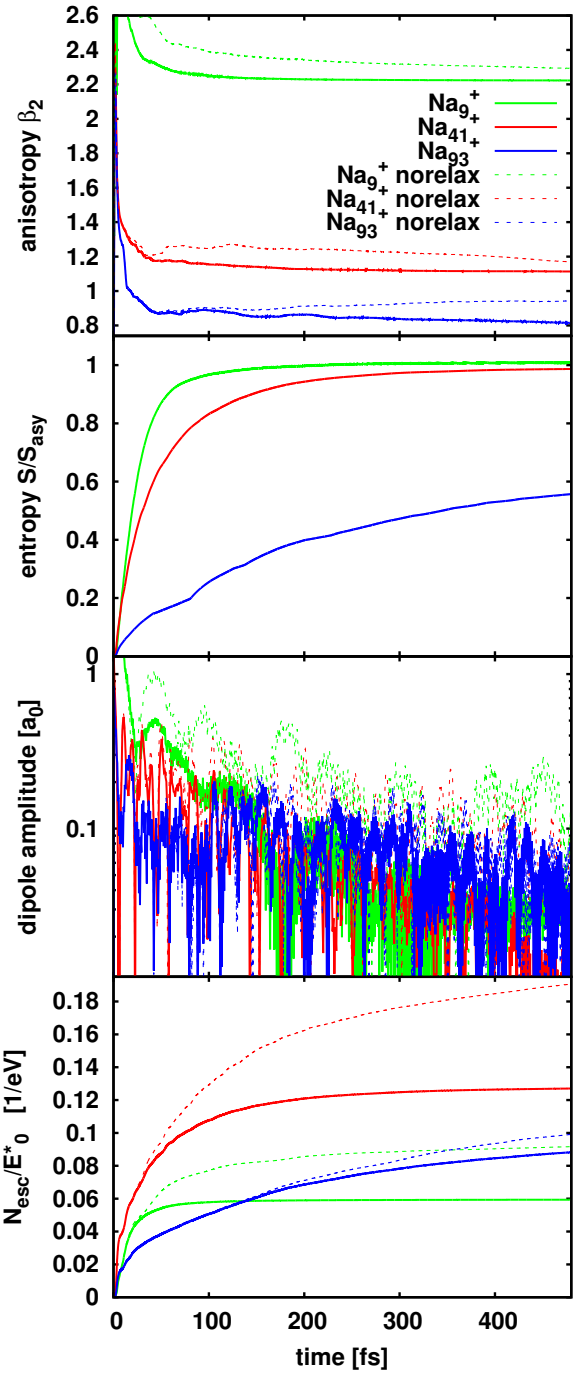

Figure 5: (Color online) Same as Fig. 3, but for varied cluster size comparing Na_9^+, Na_{41}^+, and Na_{93}^+. Boost energy is in all cases $E_0^* = 2.7$ eV.

C. Laser excitation

Having explored the basic features of RTA for in terms of the simple boost excitation, we now present a quick first exploration of laser excitations. The laser field is described as a classical electro-magnetic wave handled in the limit of long wavelengths. This amounts to add to

TDLDA a time-dependent external dipole field

$$U_{\rm ext}(\mathbf{r},t) \;=\; e^2\mathbf{r}\cdot\mathbf{e}_{\rm z}\,E_0\,f(t)\,\sin(\omega_{\rm las}t) \quad , \qquad (15a)$$

$$f(t) \;=\; \sin^2\left(\pi\frac{t}{T_{\rm pulse}}\right)\theta(t)\theta(T_{\rm pulse}-t) \qquad (15b)$$

The laser features therein are: the (linear) polarization $\mathbf{e}_{\rm z}$ along the symmetry axis, the peak field strength E_0 related to laser intensity as $I_0 \propto E_0^2$, photon frequency $\omega_{\rm las}$, and pulse length $T_{\rm pulse}$. Actually we use $T_{\rm pulse} =$ 96 fs corresponding to a Full-Width at Half Maximum (FWHM) of 48 fs for field strength.

In order to track the energy balance in the process, we use here two energetic observables: first the energy absorbed from the laser field

$$E_{\rm exc} = \int_0^t dt' \int d^3r\,\varrho(\mathbf{r},t')\partial_{t'}U_{\rm ext}(\mathbf{r},t') \qquad (16)$$

where ϱ is the usual electron density, and second, the intrinsic kinetic energy $E^*_{\rm intr}$ (Eq. (C1)), see appendix C.

Figure 6 shows results for a laser intensity $I = 10^{10}$W/cm^2. Calculations were done up to time 250 fs for a set of laser frequencies. Shown in panels b–e are the asymptotic values of the observables which are practically reached at this final time. Panel a shows for comparison the dipole strength distribution obtained from spectral analysis after small boost (linear regime). The frequency dependence of ionization (panel e) maps roughly the dipole strength distribution (compare with panel a and mind that the present scan of $\omega_{\rm las}$ has low resolution). Relaxation suppresses ionization considerably at the peaks of the distribution, i.e. for resonant excitation. Practically no dissipative effects are seen in the off-resonant minima between the peaks and in the region above IP. Absence of dissipation is related to an emission process faster than the relaxation time. This is obvious for the energies above IP. These are direct emission processes which run for Na clusters at a time scale of few fs [13, 28]. Very instructive is the different behavior for on- and off-resonant processes below IP. Resonant excitations are known to oscillate for a longer amount of time [58] which, in turn, gives dissipation long time to interfere. Off-resonant excitations, even if they involve multi-photon processes, are confined to short times. The photons involved have to cooperate instantaneously.

The intrinsic kinetic energy $E^*_{\rm intr}$ shown in panel c of Figure 6 complements the information from ionization. No differences between TDLDA and RTA are seen for the off-resonant processes while resonant processes shift a larger part of the excitation energy to $E^*_{\rm intr}$, that part being thus lost for direct ionization. It is interesting to note that the total excitation energy $E_{\rm exc}$ absorbed from the laser (panel d) is practically the same with and without relaxation term. It is the balance between intrinsic excitation (thermalization) and direct ionization which is regulated by the relaxation term. As expected, anisotropy β_2 (panel b) is visibly lowered for all resonant processes where dissipation is at work. A similar effect had been see in previous study using VUU [59].

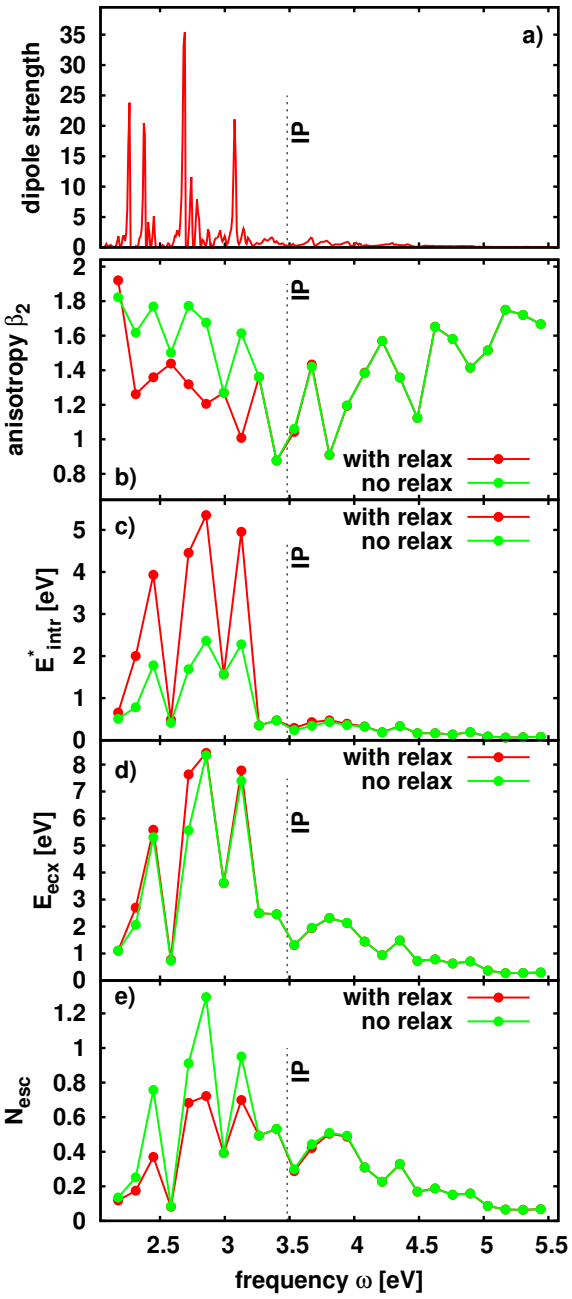

Figure 6: (Color online) Asymptotic values of four key observables after laser excitation with a laser pulse of intensity $I = 10^{10}$W/cm^2, pulse with sin^2 profile of duration $T_{\rm pulse} = 96$ fs (thus FWHM=48 fs), and varying frequency (drawn along x axis). Test case is Na_{40} with ionic background in CAPS. The observables are: e) ionization $N_{\rm esc}$, d) excitation energy deposited by the laser $E_{\rm exc}$, c) intrinsic (thermal) kinetic energy $E^*_{\rm intr}$ and b) anisotropy β_2 of the angular distribution of emitted electrons, and entropy. Compared are results from RTA (using the standard scattering cross section 6.5 a$_0^2$) and TDLDA without relaxation. The uppermost panel a) shows for comparison the spectral distribution of dipole strength computed from an instantaneous boost (see section IV B 1).

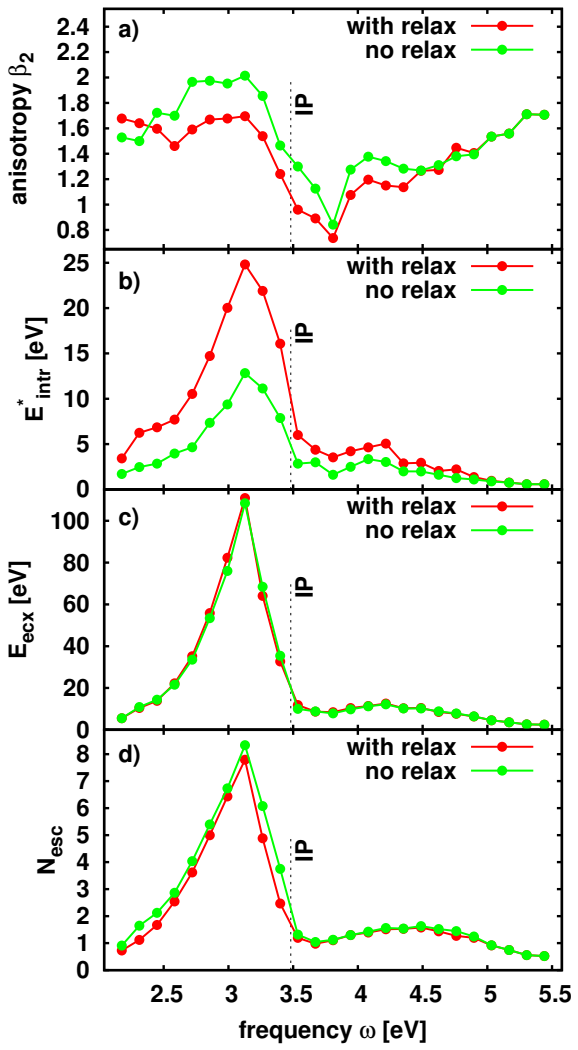

Figure 7: (Color online) Asymptotic values of four key observables after laser excitation with a laser pulse of intensity $I = 10^{11}\mathrm{W/cm^2}$, pulse with $\sin^2$ profile of duration $T_{\mathrm{pulse}} = 96$ fs (thus FWHM=48 fs), and varying frequency (drawn along x axis). Test case is Na_{40} with ionic background in CAPS. The observables are: d) ionization N_{esc}, c) excitation energy E_{exc} absorbed from the laser, b) intrinsic (thermal) kinetic energy E^*_{intr}, a) anisotropy β_2 of the angular distribution of emitted electrons. Compared are results from calculations with RTA (using the standard scattering cross section 6.5 $\mathrm{a_0^2}$) and without.

Figure 7 shows results for a higher laser intensity $I = 10^{11}\mathrm{W/cm^2}$. The pattern are much different from the previous case. Ionization (panel d) shows one broad resonance peak. This happens already for TDLDA because ionization acts here as a strong dissipation mechanism [60]. In fact, ionization is always fast in this regime of violent excitations and thus always the dominant mechanism. Little is left to do for collisional relaxation. The energy absorption (panel c) is huge and, of course, shows no difference with and without relaxation term. The effect of dissipation is seen more clearly in the intrinsic energy (panel b). The ratio between the full calculation and pure TDLDA amounts to about a factor two. Mind, however, that this is a large difference on a small quantity. In any case, only a small fraction of the total absorbed energy (panel c) is moved into intrinsic excitation and 80% or 90% are eaten up for ionization. The E^*_{intr} shows another feature which seems surprising at first glance: a difference between RTA calculation and TDLDA persists in some region above the IP. This has a simple explanation. The strong ionization enhances the IP in the course of the dynamics. Thus the system sees in the average a larger IP than in the ground state and this shifts the regime of purely direct processes to higher laser intensity. The fact that somewhat more of the absorbed energy is moved into intrinsic excitation is also reflected by the anisotropy (panel a) which is reduced as compared to TDLDA up the point where E^*_{intr} differs.

After all, these two short examples indicate that the interplay of laser excitation and collisional relaxation carries a world of interesting effects waiting to be uncovered. This calls for further studies.

V. CONCLUSIONS

In this paper, we have proposed a practical way to include collisional correlations in finite fermion systems at a quantum mechanical level. The issue is crucial for energetic processes in many systems from nuclei to clusters and molecules. Our approach is inspired from the semi-classical picture, but remains strictly quantum mechanical. It relies on a Relaxation Time Approximation (RTA) of the quantum collision term. The key ingredients of our RTA are the instantaneous equilibrium density matrix $\hat{\rho}_{\mathrm{eq}}(t)$ and the instantaneous relaxation time $\tau_{\mathrm{relax}}(t)$. The scheme is applicable to any finite fermion system. It turns out to be efficient and robust in various dynamical scenarios.

As typical application we have investigated simple metal clusters subject to a possibly strong electromagnetic perturbation (collision with by-passing ion or laser irradiation). Inclusion of dissipation through RTA provides the expected behaviors: enhanced damping of oscillations, reduced ionization, more energy transfer to intrinsic degrees of freedom (electronic thermalization), and more isotropic emission of electrons. The effects strongly depend on excitation conditions and strengths (boost amplitude, laser frequency or intensity) which is very plausible. For the given collision rates used in our RTA, we find a strong competition between collisional relaxation and damping through direct electron emission whose outcome depends sensitively on the actual dynamical conditions. RTA becomes particularly beneficial for resonant laser excitations. In this case, pure TDLDA is plagued by long lasting oscillations of the system which are unphysical. RTA yields a realistic attenuation of the dipole signal.

The present RTA provides a valuable extension of

mean field theories such as the LDA version of DFT for energetic dynamical scenarios requiring a proper account of dissipation. Although RTA is restricted to situations which can be modeled by one global (but instantaneous) relaxation rate it certainly provides a valuable step in the right direction. It surely deserves further exploration end extension to other observables as, e.g., the widely explored photo-electron spectra. Work along that line is in progress.

Acknowledgments

We thank Thomas Fennel for helpful discussions. We thank the RRZE (Regionales Rechenzentrum Erlangen) for supplying the computing resources for the studies presented here. We also thank Institut Universitaire de France, ITN network CORINF and french ANR Muses program for financial support.

Appendix A: Solution of the RTA equations

1. Interlaced mean-field and RTA time steps

For completeness we remind the RTA equation (11)

$$\partial_t \hat{\rho} \;=\; -\mathrm{i}\big[\hat{h},\hat{\rho}\big] - \frac{1}{\tau_{\rm relax}}\left(\hat{\rho} - \hat{\rho}_{\rm eq}[\hat{\rho}]\right) \quad ,$$

Its r.h.s. contains first the term (1) driving mean-field propagation and second the dissipative term. Mean-field propagation covers all s.p. oscillations and runs at a much faster pace than relaxation. We thus treat the two contributions at different time scales. The dissipative term is evaluated in time steps of Δt (thus at discrete times $t_n = n\Delta t$), while the mean-field propagation (12a) is resolved on a finer mesh δt. To make the dependencies more transparent, we express the instantaneous equilibrium density more generally as $\hat{\rho}_{\rm eq}[\hat{\rho}]$, i.e. as functional of given density operator $\hat{\rho}$ which is communicated through the local density, current, and energy of $\hat{\rho}$.

Formally, we express the higher resolution for the mean-field propagation in terms of the evolution operator (2a) and use that to transform to the interaction picture. During the step from $t_n = n\Delta t$ to $t_{n+1} = (n+1)\Delta t$ we thus map

$$\tilde{\rho}(t) \;=\; \hat{U}^{-1}(t,t_n)\hat{\rho}(t)\hat{U}(t,t_n)\;, \tag{A1a}$$
$$\hat{\rho}(t) \;=\; \hat{U}(t,t_n)\tilde{\rho}(t)\hat{U}^{-1}(t,t_n)\;, \tag{A1b}$$

which turns Eq. (11) into

$$\partial_t \tilde{\rho} \;=\; -\frac{1}{\tau_{\rm relax}}\left(\tilde{\rho} - \tilde{\rho}_{\rm eq}[\hat{\rho}]\right) \quad .$$

Integrating time over the interval $[t_n, t_{n+1}]$ yields

$$\begin{aligned}\tilde{\rho}(t_{n+1}) \;&=\; \tilde{\rho}(t_n) - \int_{t_n}^{t_{n+1}} dt'\,\frac{\tilde{\rho}(t') - \tilde{\rho}_{\rm eq}[\hat{\rho}(t')]}{\tau_{\rm relax}} \\ &\approx\; \tilde{\rho}(t_n) - \frac{\Delta t}{\tau_{\rm relax}}\left[\tilde{\rho}(t_{n+1}) - \tilde{\rho}_{\rm eq}[\hat{\rho}(t_{n+1})]\right]\end{aligned}$$

where the last step represents a perturbative evaluation of the dissipation in the time interval $[t_n, t_{n+1}]$. Using Eq. (A1b), we transform back into the Schrödinger picture to

$$\hat{\rho}(t_{n+1}) \;=\; \hat{\rho}_{\rm mf} - \frac{\Delta t}{\tau_{\rm relax}}\left[\hat{\rho}_{\rm mf} - \hat{\rho}_{\rm eq}[\hat{\rho}_{\rm mf}]\right]\;, \tag{A2a}$$
$$\hat{\rho}_{\rm mf} \;=\; \hat{U}(t_{n+1},t_n)\hat{\rho}(t_n)\hat{U}^{-1}(t_{n+1},t_n) \tag{A2b}$$

with all terms now expressed at time t_{n+1}. This equation delivers the stepping scheme. We first perform a mean-field propagation in standard manner from t_n to t_{n+1}. This yields the propagated $\hat{\rho}_{\rm mf}$. We then compute the corresponding $\hat{\rho}_{\rm eq}[\hat{\rho}_{\rm mf}] \equiv \hat{\rho}_{\rm eq}[\varrho_{\rm mf}, \mathbf{j}_{\rm mf}, E_{\rm mf}]$, and use that finally to compose the relaxation step (A2a).

2. Estimate of the relaxation time

We refer to a semi-classical estimate of relaxation rates developed in [61] for homogeneous nuclear matter. Rescaling that from the nuclear spin-isospin degeneracy factor $g = 4$ to the electronic spin degeneracy $g = 2$, we obtain as starting point

$$\frac{\hbar}{\tau_{\rm relax}} = 3.95\frac{\hbar^2}{m}\sigma_{ee}k_{\rm F}\rho_0\frac{T^2}{\varepsilon_{\rm F}^2} \tag{A3}$$

where m is the electron mass, $k_{\rm F}$ the Fermi momentum, ρ_0 the matter density, $\varepsilon_{\rm F}$ the Fermi energy, and σ_{ee} the effective in-medium cross section for electron-electron collisions. Using the standard relations for a degenerate electron gas, $r_s = 1.92/k_{\rm F}$, $\varepsilon_{\rm F} = 3.68/r_s^2$, and $\rho_0 = 3/(4\pi r_s^3)$ (see [62]), we obtain

$$\frac{\hbar}{\tau_{\rm relax}} = 0.133\frac{\hbar^2}{m}\sigma_{ee}T^2 \quad . \tag{A4}$$

It is preferable to express the rate in term of the intrinsic thermal excitation energy [61, 62]

$$\frac{E^*_{\rm intr}}{N} = \frac{\pi^2 T^2}{4\varepsilon_{\rm F}} \tag{A5}$$

where N is the actual particle number. A word of caution is necessary here. We are working in a system with absorbing boundary conditions to account for ionization. This means that the number of particles is a time dependent quantity. The value N is the one characterizing the system at a given instant and thus time dependent. We resolve the above expression to T and express again $\varepsilon_{\rm F}$ through r_s. This yields finally Eq. (13), i.e.

$\hbar/\tau_{\rm relax} = 0.40 E^*_{\rm intr}\sigma_{ee}/(N r_s^2)$. The intrinsic excitation energy $E^*_{\rm intr}$ is a dynamical observable which has to be determined anew at each time step, for details see Appendix C.

The Wigner-Seitz radius r_s is a crucial parameter in the estimate of the relaxation time. It characterizes the average electron density and it is naturally given in the case of the jellium model. For a cluster with detailed ionic background, there are two ways to deduce r_s from the given cluster. One can take either the electronic diffraction radius $R_{\rm el,diffr}$ (box equivalent radius) as defined in [63] and identify

$$r_s = R_{\rm el,diffr} N^{-1/3} \tag{A6a}$$

or one can take the ionic r.m.s. radius $r_{\rm ion}$ which is often simpler to evaluate. The ionic structure has practically no surface zone and thus the ionic diffraction radius is $R_{\rm el,diffr} = \sqrt{3/5} r_{\rm ion}$. We know that the electron distribution in metals follows closely the ionic background due to the strong, attractive Coulomb interaction. This allows to identify alternatively

$$r_s = \sqrt{\frac{3}{5}}\, r_{\rm ion} N^{-1/3} \quad . \tag{A6b}$$

Both definitions yield in practice very similar results. We use the form (A6b) which is simpler to handle, particularly in case where the ionic structure is frozen. In practice, it is sufficiently well described by a constant $r_s = 3.7$ a_0.

It remains to determine the effective cross section σ_{ee}. We use here the careful evaluation of [64, 65]. They compute electron screening for homogeneous electron matter in Thomas-Fermi approximation, compute from that the scattering cross-section and apply a Pauli correction of factor 1/2. This yields $\sigma_{\rm ee} = 6.5$ a_0^2 for the case of Na clusters at $r_s \approx 3.7$ a_0. It is this value which was used as reference throughout this paper.

Appendix B: Density Constrained Mean-Field (DCMF)

A key task is to determine the instantaneous equilibrium density-operator $\hat\rho_{\rm eq}[\varrho, \mathbf{j}, E]$ in the RTA equation (11). It is the mean-field state of minimum energy under the constraints of given local density ϱ, current $\mathbf{j}$, and energy E. A scheme for density constrained mean-field (DCMF) calculations was developed in [66]. We use it here in a version extended to account also for the constraint on current $\mathbf{j}(\mathbf{r})$. The density constrained mean-field Hamiltonian then reads

$$\begin{aligned} \hat h_{\rm dens.co.}[\varrho] \;=\; \hat h_{mf}[\varrho] &- \int d^3r\, \lambda_\varrho(\mathbf{r})\hat\varrho(\mathbf{r}) \\ &- \int d^3r\, \boldsymbol{\lambda_j}(\mathbf{r})\hat{\mathbf{j}}(\mathbf{r}) \end{aligned} \tag{B1}$$

where $\hat h_{mf}[\varrho]$ is the standard mean-field Hamiltonian for the given local density $\varrho(\mathbf{r})$, $\hat\varrho(\mathbf{r})$ is the operator of local density, $\hat{\mathbf{j}}(\mathbf{r})$ the operator of local current, while λ_ϱ and $\boldsymbol{\lambda_j}$ stand for the associated Lagrange parameters. These are determined iteratively such that the solution of the corresponding Kohn-Sham equations yields the wanted density $\varrho(\mathbf{r})$ and current $\mathbf{j}(\mathbf{r})$ [66].

As a further constraint, we want to adjust the equilibrium state to given energy $E_{\rm goal} = E_{\rm mf} = E[\hat\rho]$ and particle number $N_{\rm goal}$. $N_{\rm goal}$ represents the actual number of particles in the system, also denoted N in the core of the text of the paper. Its computation is simple. It is just given by the integral over the computational box of the density $\varrho(\mathbf{r})$ at a given RTA time step t_n. The adjustment of $E_{\rm goal}$ and $N_{\rm goal}$ is achieved by considering a thermalized mean-field state $\hat\rho_{\rm eq}$ of the form Eq. (3) where each s.p. state ϕ_α is augmented with an occupation weight

$$W_\alpha^{\rm (eq)} \;=\; \frac{1}{1+\exp\left((\varepsilon_\alpha-\mu)/T\right)}\,, \tag{B2a}$$

$$(\mu, T) \;\leftrightarrow\; {\rm tr}\{\hat\rho_{\rm eq}\} = N_{\rm goal}\,,\; E[\hat\rho_{\rm eq}] = E_{\rm goal}\,. \tag{B2b}$$

Temperature T and chemical potential μ are to be adjusted such that the wanted total particle number $N_{\rm goal}$ and energy $E_{\rm goal}$ is reproduced. To simplify the computations, the occupation numbers are adjusted to the Fermi form (B2a) once before DCMF and once after the DCMF iterations. The final reoccupation after DCMF slightly spoils the reproduction of density and current. But the deviations remain small along all time propagation.

Appendix C: The intrinsic excitation energy

DCMF is also used to compute the intrinsic excitation energy $E^*_{\rm intr}$ which is, in fact, the intrinsic kinetic energy. The total kinetic energy is the difference between the actual energy E and the minimal energy at given local density $\varrho(\mathbf{r})$ which is the energy of the (stationary) DCMF state for fixed $\varrho(\mathbf{r})$, $\mathbf{j} = 0$ and $T = 0$. Part of the total kinetic energy goes into the kinetic energy of the collective flow represented by $\mathbf{j}(\mathbf{r})$. The other part is the intrinsic kinetic energy $E^*_{\rm intr}$. We evaluate it by computing the DCMF state for given $\varrho(\mathbf{r})$, $\mathbf{j}(\mathbf{r}) \neq 0$, but now for $T = 0$ to find the minimum energy $E_{\rm DCMF}[\varrho(\mathbf{r}), \mathbf{j}(\mathbf{r}), T{=}0]$ under the given constraints. The difference between total energy and this energy is then the intrinsic kinetic energy

$$E^*_{\rm intr} = E - E_{\rm DCMF}[\varrho(\mathbf{r}), \mathbf{j}(\mathbf{r}), T{=}0] \quad . \tag{C1}$$

This fully quantum-mechanical definition is used for estimating the relaxation time in Eq. (13) which is a crucial parameter in the propagation. For analyzing purposes (see section IV C), we can use the less expensive semiclassical Thomas-Fermi approximation for $E_{\rm kin,DCMF}$ as done in previous works [13, 28].

Appendix D: Mixing of two one-body density matrices

The dissipative step delivers a density matrix (A2a) which is a mix

$$\begin{aligned}\hat{\rho}(t_{n+1}) &= (1-\eta)\,\hat{\rho}_{\rm mf} + \eta\hat{\rho}_{\rm eq}\ ,\ \eta = \frac{\Delta t}{\tau_{\rm relax}}\ ,\\ \hat{\rho}_{\rm mf} &= \sum_\alpha |\phi_\alpha^{\rm (mf)}\rangle W_\alpha \langle\phi_\alpha^{\rm (mf)}|\ ,\\ \hat{\rho}_{\rm eq} &= \sum_\alpha |\phi'_\alpha\rangle W'_\alpha \langle\phi'_\alpha|\ ,\end{aligned}$$

where the $|\phi_\alpha^{\rm (mf)}\rangle = \hat{U}(t_{n+1},t_n)|\phi_\alpha(t_n)\rangle$ constitute the basis of TDLDA-propagated states while the $|\phi'_\alpha\rangle$ are new states from DCMF which also delivers new occupancies W'_α. We expand the composed state $\hat{\rho}(t_{n+1})$ with respect to the set $\{|\phi_\alpha^{\rm (mf)}\rangle\}$ because it represents the majority contribution. It reads

$$\begin{aligned}&\hat{\rho}(t_{n+1}) = \sum_{\alpha\beta} |\phi_\alpha^{\rm (mf)}\rangle \rho_{\alpha\beta} \langle\phi_\beta^{\rm (mf)}|\ ,\\ &\rho_{\alpha\beta} = (1-\eta)\delta_{\alpha\beta}W_\alpha + \eta\sum_\gamma \langle\phi_\alpha^{\rm (mf)}|\phi'_\gamma\rangle W'_\gamma \langle\phi'_\gamma|\phi_\beta^{\rm (mf)}\rangle\ .\end{aligned}$$

For the further propagation, we want to use again the diagonal representation (3). To this end, we diagonalize $\rho_{\alpha\beta}$ which finally delivers the new set $|\phi_\alpha(t_{n+1})\rangle$ and $W_\alpha(t_{n+1})$ which will remain constant over the next RTA step from t_{n+1} to t_{n+2}.

Appendix E: Iterative correction of particle number and energy

After mixing (A2a), one may end up with a slight deviation from the wanted energy $E_{\rm goal}$ although we have taken care that both entries as such meet this energy (see section B). But minimal energy violations may accumulate during long propagation. The task is thus to correct for a possibly occuring, small energy error

$$\delta E = E(\hat{\rho}_{\rm mix}) - E_{\rm goal} \tag{E1}$$

where $E(\hat{\rho}_{\rm mix})$ is the actual total energy after the mixing step. We need a scheme to correct the total energy with as little modification as possible. To this end, we may employ an iterative strategy. We avoid direct use of the equilibrium distribution and express a corrective step in terms of the given occupation numbers W_α. To this end, we take over from the equilibrium distribution the crucial property

$$\delta W_\alpha^{\rm (equi)} = -\left(\delta T\frac{\varepsilon_\alpha-\mu}{T^2} + \delta\mu\frac{1}{T}\right) W_\alpha^{\rm (equi)}\big(1-W_\alpha^{\rm (equi)}\big)\quad . \tag{E2}$$

We take this as motivation to postulate for a general change

$$\delta W_\alpha = (\delta_1\varepsilon_\alpha + \delta_0)\, W_\alpha(1-W_\alpha)\quad . \tag{E3}$$

The δ_i are tuned to desired change in particle number δN and in energy δE (where δE is determined from the energy loss in the relaxation step). The conditions to fulfill are

$$\sum_\alpha \delta W_\alpha = 0\quad ,\quad \sum_\alpha \varepsilon_\alpha \delta W_\alpha = \delta E\quad .$$

The energy conservation is formulated in terms of the s.p. energies. This is valid in the linear regime because of

$$E(\hat{\rho}+\delta\hat{\rho}) = E(\hat{\rho}) + {\rm tr}\{\hat{h}\delta\hat{\rho}\} = E(\hat{\rho}) + \sum_\alpha \delta W_\alpha \varepsilon_\alpha\quad .$$

Thus we want to fulfill

$$\sum_\alpha \delta W_\alpha = \delta N \ = \ \delta_0\overline{1} + \delta_1\overline{\varepsilon}\quad , \tag{E4a}$$

$$\sum_\alpha \delta W_\alpha\varepsilon_\alpha = \delta E \ = \ \delta_0\overline{\varepsilon} + \delta_1\overline{\varepsilon^2}\quad , \tag{E4b}$$

with $\overline{A} = \sum_\alpha w_\alpha(1-w_\alpha)A_\alpha$. This linear system is resolved by

$$\delta_0 = \frac{\overline{\varepsilon^2}\delta N - \overline{\varepsilon}\delta E}{\overline{\varepsilon^2}\,\overline{1} - (\overline{\varepsilon})^2}\quad , \tag{E5a}$$

$$\delta_1 = \frac{-\overline{\varepsilon}\delta N + \overline{1}\delta E}{\overline{\varepsilon^2}\,\overline{1} - (\overline{\varepsilon})^2}\quad . \tag{E5b}$$

Thus we obtain the δ_i and subsequently the δW_α according to eq. (E3). Finally, it has to be checked whether the readjusted density matrix $\hat{\rho}_{\rm mix,cor} = \sum_\alpha |\phi_\alpha\rangle(W_\alpha + \delta W_\alpha)\langle\phi_\alpha|$ fulfills $E(\hat{\rho}_{\rm mix,cor}) = E_{\rm goal}$. In case, the energy matching is not good enough, the above stepping has to be repeated.

[1] T. Wada, N. Carjan, and Y. Abe, Nucl. Phys. A **538**, 283 (1992).

[2] Y. Abe, S. Ayik, P.-G. Reinhard, and E. Suraud, Phys. Rep. **275**, 49 (1996).

[3] U. Saalmann, C. Siedschlag, and J. M. Rost, Journal of Physics B **39** (2006).

[4] T. Fennel, , K.-H. Meiwes-Broer, J. Tiggesbäumker, P.-G. Reinhard, P. M. Dinh, and E. Suraud, Rev. Mod. Phys. **82**, 1793 (2010).

[5] J. Dalibard, in *Proceedings of the International School of Physics-Enrico Fermi, Course CXL*, edited by M. Inguscio, S. Stringari, and C. Wieman (IOS Press, Amsterdam,

1999), p. 321.
[6] G. Chen, *Nanoscale Energy Transport and Conversion: A Parallel Treatment of Electrons, Molecules, Phonons, and Photons* (Oxford University Press, New York, 2005).
[7] M. Kjellberg, O. Johansson, F. Jonsson, A. V. Bulgakov, C. Bordas, E. E. B. Campbell, and K. Hansen, Phys. Rev. A **81**, 023202 (2010).
[8] P. Wopperer, C. Z. Gao, T. Barillot, C. Cauchy, A. Marciniak, V. Despré, V. Loriot, G. Celep, C. Bordas, F. Lépine, et al. (2014), submitted.
[9] J. Pinaré, B. Baguenard, C. Bordas, and M. Broyer, Eur. Phys. J. D **9**, 21 (1999).
[10] E. K. U. Gross and W. Kohn, Adv. Quant. Chem. **21**, 255 (1990).
[11] E. K. U. Gross, J. F. Dobson, and M. Petersilka, Top. Curr. Chem. **181**, 81 (1996).
[12] M. A. L. Marques, N. T. Maitra, F. M. S. Nogueira, E. K. U. Gross, and A. Rubio, *Fundamentals of Time-Dependent Density Functional Theory* (Lect. Notes in Phys. vol 837,Springer-Verlag, Berlin, 2012).
[13] F. Calvayrac, P.-G. Reinhard, E. Suraud, and C. A. Ullrich, Phys. Rep. **337**, 493 (2000).
[14] M. A. Marques, C. A. Ullrich, F. Nogueira, A. Rubio, K. Burke, and E. K. Gross, *Time Dependent Density Functional Theory* (Springer, Berlin, 2006).
[15] L. P. Kadanoff and G. Baym, *Quantum Statistical Mechanics: Green's Function Methods in Equilibrium and Nonequilibrium Problems* (Frontiers in physics, Benjamin, New York, 1962).
[16] C. Cercignani, *The Boltzmann equation and its applications* (Applied Mathematical Sciences 67, Springer, New York, 1988).
[17] E.-A. Uehling and G.-E. Uhlenbeck, Phys. Rev. **43**, 552 (1933).
[18] G. F. Bertsch and S. Das Gupta, Phys. Rep. **160**, 190 (1988).
[19] D. Durand, E. Suraud, and B. Tamain, *Nuclear Dynamics in the Nucleonic Regime* (Institute of Physics, London, 2000).
[20] A. Domps, P.-G. Reinhard, and E. Suraud, Phys. Rev. Lett. **81**, 5524 (1998).
[21] T. Fennel, G. F. Bertsch, and K.-H. Meiwes-Broer, Eur. Phys. J. D **29**, 367 (2004).
[22] P. Ring and P. Schuck, *The Nuclear Many-Body Problem* (Springer, Berlin, 1980).
[23] K. Hansen, *Statistical physics of nanoparticles in the gas phase* (Springer Netherlands, Amsterdam, 2013).
[24] F. Calvayrac, A. Domps, S. El-Gammal, C. Kohl, P.-G. Reinhard, and E. Suraud, in *Proceedings of Intern. Conf. NuCl Prag 97* (Czech. Journ. Phys, 1998), vol. 48, p. 715.
[25] C. Legrand, E. Suraud, and P.-G. Reinhard, J. Phys. B **35**, 1115 (2002).
[26] P. Klüpfel, P. M. Dinh, P.-G. Reinhard, and E. Suraud, Phys. Rev. A **88**, 052501 (2013).
[27] R. M. Dreizler and E. K. U. Gross, *Density Functional Theory: An Approach to the Quantum Many-Body Problem* (Springer-Verlag, Berlin, 1990).
[28] P.-G. Reinhard and E. Suraud, *Introduction to Cluster Dynamics* (Wiley, New York, 2004).
[29] D. Pines and P. Nozières, *The Theory of Quantum Liquids* (W A Benjamin, New York, 1966).
[30] P. L. Bhatnagar, E. P. Gross, and M. Krock, Phys. Rev. **94**, 1954 (511).
[31] N. W. Ashcroft and N. D. Mermin, *Solid State Physics* (Saunders College, Philadelphia, 1976).
[32] E. M. Lifschitz and L. P. Pitajewski, *Physikalische Kinetik*, vol. X of *Lehrbuch der Theoretischen Physik* (Mir, Moscow, 1988).
[33] K. Gütter, P.-G. Reinhard, and C. Toepffer, Phys. Rev. A **38**, 1641 (1988).
[34] S. Kohler, Nucl. Phys. A **343**, 315 (1980).
[35] S. Kohler, Nucl. Phys. A **378**, 181 (1982).
[36] C. Y. Wong and K. T. R. Davies, Phys. Rev. C **28**, 240 (1983).
[37] H. Reinhardt, P.-G. Reinhard, and K. Goeke, Phys. Lett. B **151**, 177 (1985).
[38] K. Goeke, P.-G. Reinhard, and H. Reinhardt, Ann. Phys. (N.Y.) **166**, 257 (1986).
[39] P.-G. Reinhard, P. D. Stevenson, D. Almehed, J. A. Maruhn, and M. R. Strayer, Phys. Rev. E **73**, 036709 (2006).
[40] S. Kümmel, M. Brack, and P.-G. Reinhard, Eur. Phys. J. D **9**, 149 (1999).
[41] B. Montag and P.-G. Reinhard, Phys. Lett. A **193**, 380 (1994).
[42] B. Montag and P.-G. Reinhard, Z. Phys. D **33**, 265 (1995).
[43] K. T. R. Davies and S. E. Koonin, Phys. Rev. **C23**, 2042 (1981).
[44] M. D. Feit, J. A. Fleck, and A. Steiger, J. Comp. Phys. **47**, 412 (1982).
[45] V. Blum, G. Lauritsch, J. A. Maruhn, and P.-G. Reinhard, J. Comp. Phys **100**, 364 (1992).
[46] J. P. Perdew and Y. Wang, Phys. Rev. B **45**, 13244 (1992).
[47] F. Calvayrac, P.-G. Reinhard, and E. Suraud, Ann. Phys. (N.Y.) **255**, 125 (1997).
[48] A. Pohl, P.-G. Reinhard, and E. Suraud, Phys. Rev. A **70**, 023202 (2004).
[49] P.-G. Reinhard and E. Suraud, in *Time-dependent density functional theory*, edited by M. A. L. Marques, C. A. Ullrich, and F. Nogueira (Springer, Berlin, 2006), vol. 706 of *Lecture Notes in Physics*, p. 391.
[50] P. Wopperer, B. Faber, P. M. Dinh, P.-G. Reinhard, and E. Suraud, Phys. Lett. A **375**, 39 (2010).
[51] P. Wopperer, B. Faber, P. M. Dinh, P.-G. Reinhard, and E. Suraud, Phys. Rev. A **82**, 063416 (2010).
[52] L. E. Reichl, *A Modern Course in Statistical Physics* (Wiley, New York, 1998).
[53] M. Brack, Rev. Mod. Phys. **65**, 677 (1993).
[54] M. Bär, B. Jakob, P.-G. Reinhard, and C. Toepffer, Phys. Rev. A **73**, 022719 (2006).
[55] P. Wopperer, P. M. Dinh, P.-G. Reinhard, and E. Suraud, Phys. Rep. **to appear** (2014), arXiv:1407.4965.
[56] P. Wopperer, C. Z. Gao, T. Barillot, C. Cauchy, A. Marciniak, V. Despré, V. Loriot, G. Celep, C. Bordas, F. Lépine, et al., preprint (2014).
[57] P.-G. Reinhard, S. Weisgerber, O. Genzken, and M. Brack, Lecture Notes in Physics **404**, 254 (1992).
[58] P.-G. Reinhard, F. Calvayrac, C. Kohl, S. Kümmel, E. Suraud, C. A. Ullrich, and M. Brack, Eur. Phys. J. D **9**, 111 (1999).
[59] E. Giglio, P.-G. Reinhard, and E. Suraud, Phys. Rev. A **67**, 043202 (2003).
[60] C. A. Ullrich, P.-G. Reinhard, and E. Suraud, Phys. Rev. A **57**, 1938 (1998).
[61] G. Bertsch, Z. Phys. A **289**, 103 (1978).
[62] J. Maruhn, P.-G. Reinhard, and E. Suraud, *Simple mod-*

els of many-fermions systems (Springer, Berlin, 2010).
[63] J. Friedrich and N. Vögler, Nucl. Phys. A **373**, 192 (1982).
[64] J. Köhn, R. Redmer, K.-H. Meiwes-Broer, and T. Fennel, Phys. Rev. A **77**, 033202 (2008).
[65] J. Köhn, R. Redmer, and T. Fennel, New J. Phys. **14**, 055011 (2012).
[66] R. Cusson, P.-G. Reinhard, J. Maruhn, W. Greiner, and M. Strayer, Z. Phys. A **320**, 475 (1985).